Hydrodynamics and bed morphological characteristics around a boulder in a gravel stream

Xu Zexing, Zhang Chenling, Yao Qiang, Wang Xiekang and Yan Xufeng

ABSTRACT

This paper presents experimental studies on hydrodynamics and bed morphological characteristics under varying water and sediment discharges over a gravel channel bed with a boulder. Firstly, flow characteristics over a non-eroded bed with a mild slope were investigated. Results show that along the transect line located one diameter away from the boulder centerline, the existence of the boulder has negligible impact on the mean flow characteristics, which are similar to flows over a flat bed. At the boulder centerline, the flow is largely deflected by the boulder and turbulence characteristics in the horizontal plane are largely enhanced in the wake of the boulder. Secondly, water scour experiments were carried out over a steep slope. It could be observed that scour occurred around the boulder and bedloads were deposited downstream, forming a typical pool–riffle sequence. An analysis shows that the length scale (L/D) of geometric features associated with pool depth, riffle height and pool–riffle distance (S/D) are positively related to the boulder-related Froude number (Fr_b): $L/D = 1.18Fr_b - 0.11$ and $S/D = 12.5Fr_b + 0.6$; and the erosion volume (V_e) for flat bed and boulder bed is positively and negatively related to the averaged Froude number (Fr): $V_e/D^3 = 37.1Fr - 21.3$ and $V_e/D^3 = -44.8Fr - 38.6$, where D is the boulder diameter.

Key words | bed deformation, boulder bed, flow characteristics, Froude number, pool and riffle

Xu Zexing
Wang Xiekang
Yan Xufeng (corresponding author)
State Key Laboratory of Hydraulics and Mountain River Engineering,
Sichuan University,
Chengdu 610065,
China
E-mail: *xufeng.yan@scu.edu.cn*

Zhang Chenling
Ewaters Environmental Science & Technology (Shanghai) Ltd,
Shanghai, 200030,
China

Yao Qiang
College of Water Resources and Hydropower,
Sichuan University,
Chengdu 610065,
China

INTRODUCTION

Bed configurations in mountain rivers are much more complex than in plain rivers, owing to steep slopes, poorly sorted surface grains (Rickenmann 2001; Papanicolaou *et al.* 2004), wide grain size distributions, heterogeneity in bed topography, large and immobile boulders, pebble clusters, sometimes bedrock, and so on. In addition, large-size boulders are likely to be introduced onto river beds by extreme events such as torrential floods, landslides and debris flows, leading to high obstructive roughness (Zimmermann & Church 2001; Galia & Hradecký 2011). The above factors enable hydromorphodynamics in mountain rivers to largely differ from those in plain rivers (Shamloo *et al.* 2001).

IMPACTS OF BOULDERS ON HYDRODYNAMICS

In recent decades, numerous laboratory studies and field surveys have been conducted to investigate hydrodynamics around boulders. Flow obstruction by boulders narrows the flow cross-section to induce flow acceleration on both its sides while leading to a remarkable reduction of flow velocity at the upstream of the boulders (Papanicolaou *et al.* 2012; Baki *et al.* 2014, 2015). In addition, a wake region of the boulders is formed, where large amounts of eddy structures appear. This results in the readjustment of

doi: 10.2166/ws.2019.175

bed roughness, shear stress and turbulent kinetic energy (*TKE*) (Cao 1997; Strom *et al.* 2007; Lacey & Roy 2008). Flow is found to separate at the lateral edges of the boulder, leading to a downstream recirculation flow zone. The turbulence with its maximum occurs in the recirculation region, and gradually diminishes downstream of the wake region (Papanicolaou *et al.* 2012; Baki *et al.* 2014; Afzalimehr *et al.* 2019). The entire water depth around the boulder is categorized into the inner layer and the outer layer defined by the distance from the bed bottom (z/H), and the inner layer is referred to as the lower 20% of the water depth (Nezu *et al.* 1994). It is found that vertical distributions of the normalized streamwise velocity (U/u_*) and the normalized turbulence intensity (u_{rms}'/u_*) show a reasonable degree of similarity at the upstream, downstream, and both sides of the boulder (Baki *et al.* 2016). However, the mean velocity profile in the inner layer significantly deviates from the classic logarithmic profile law over flat rough beds (Papanicolaou *et al.* 2012).

IMPACTS OF BOULDERS ON BED MORPHODYNAMICS

Sediment transport is sensitive to bed surface configurations and grain size (Hassan & Church 2000). Riverbeds in steep mountain rivers always feature large roughness elements like boulders. The generated significant flow shear around such large roughness elements not only tends to result in the overestimation of sediment flux but also increases the stream power needed to transport a given amount of sediments (Lenzi *et al.* 2006; Papanicolaou *et al.* 2012; Ghilardi 2013, 2014). Original sediment transport equations often overestimate bedload flux because they cannot account for the stress borne by rarely mobile grains and differentiate between highly and minimally mobile sediment (Cui & Parker 2005; Chiari & Rickenmann 2011; Nitsche *et al.* 2011; Yager *et al.* 2012). Formulas or numerical models of sediment transport seldom consider boulder effects but pay more attention to the entrainment of bedload grains decided by bed shear stress, flow resistance or hydraulic regimes such as discharges, water level and stream power (Habersack & Laronne 2002; Barry *et al.* 2004; Schneider *et al.* 2015). To take such impacts into account, Yager *et al.* (2007) used a substitute of the median grain size of the mobile fraction to that of the whole grain seize to scale the predicted transport rate by the proportion of the bed area that is occupied by the mobile fraction, but it should be noted that the hiding effect and selective transport caused by the graded mobile sediment were ignored. Nevertheless, further studies also need to be carried out to accurately predict sediment flux and to probe its characteristics in mountain rivers.

Sediment transport and bed morphology evolution in mountain rivers are poor in comparison with the knowledge existing on lowland rivers (Ghilardi 2013) and few attempts have been presented to consider boulder effects on bedload transport (Cameron *et al.* 2017; Papanicolaou *et al.* 2018) and bed morphology evolution. The scope of this study includes two perspectives:

- The first perspective is the detailed investigation of flow characteristics in a boulder-obstructed open channel. These flow characteristics were compared with existing hydraulic knowledge in a straight open channel to understand fundamental interactions between flow and boulder.
- The second perspective aims to investigate characteristics of sediment transport and bed morphology evolution due to the existence of large-scale boulders in mountain rivers. The implication of the obtained knowledge of hydraulics and sediment dynamics in boulder-obstructed channels on the generation of pool and riffle morphologies is discussed.

METHODOLOGY

Natural mountain river survey

The natural reach surveyed is in the Baisha River, an ana-branch of the Min River located in central Sichuan province, China. The Baisha River has all its basin of an average width of ~8 km in Dujiangyan, Chengdu, as shown in Figure 1. The river contains plenty of water resources with an average annual runoff ~15.8 m^3/s. Originated from the southern foothills of Guangguang Mountain in the southern segment of the Longmen range, the Baisha River is a typical mountain river featuring a steep slope of ~4.8% and a river length of ~49.3 km. The clear water upstream of the river tends to induce the formation of an armoring layer of the

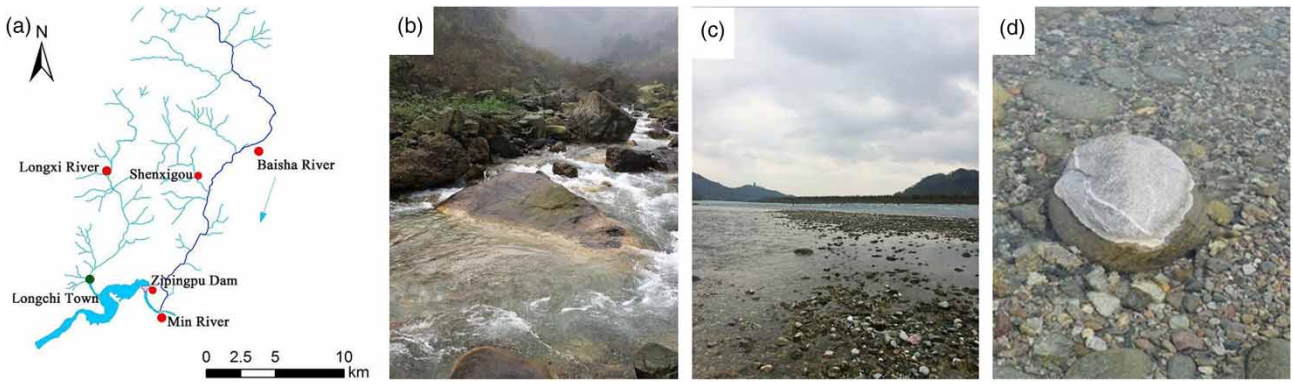

Figure 1 | Typical channel morphology and gravel bed with boulders in the Baisha River.

river bed. The survey showed that the wide size distribution of grains was identified with roughness pebbles, protrusion particles, and step–pool framework as well as large amounts of boulders. A typical survey shows that the diameter of the boulder is 0.56 m and the median diameter of gravel on the bed is roughly 0.025 m. Thus the geometric similarity represented by the ratio of boulder size to gravel size is 22.4, which is applied to designs of flume bed configurations.

Experimental measurement of hydrodynamics over a flat boulder bed

A flat rectangular flume with a total longitudinal gradient of 1‰ had a length of 16 m, width of 0.505 m, and depth of 0.4 m (Figure 2(a)). Cement was pasted on the flume bottom to mimic channel roughness. A broad crest was installed at the entrance to control water discharge. After the weir, a stilling pond was configured to dissipate water energy and a plate was used to smoothly transit flow to the flume. A tailgate was installed to adjust water depth. A 5 m-long and 0.1 m-thick sediment layer with a median diameter of $k_s = 7$ mm was placed in the central flume. At both ends of the sediment layer, 1 m-long triangular pebble patches were installed to guarantee a smooth transition of water flow. According to geometric similarity, an isolated boulder with an effective diameter of $D = 15.7$ cm was placed on the bed center.

Downlooking acoustic doppler velocimetry (ADV) was employed to measure instantaneous three-dimensional flow velocities. The vertical location of velocity measurement close to the bed was 5 cm above the sediment layer and the uppermost location was 7 cm below the free water surface due to the working configuration of the ADV. Measured data were filtered out when the correlation coefficient was less than 70%, the noise decibels were less than 15 dB, and overall confidence intervals were higher than 90% (Lacey & Roy 2006).

By fitting the coordinate with the flume, u, v and w denote time-averaged velocities in x, y and z directions. The coordinate system is nondimensionalized by effective diameter $D = 15.7$ cm for $x^+ = x/D$, $y^+ = y/D$, and by constant water depth H for $z^+ = z/H$. The origin O is fixed at the center point of the boulder. Three transverse longitudinal transects $y^+ = -1$, 0, 1 were selected for flow measurements; 5–19 verticals at the three transects were specified and 5–15 points along those verticals were measured. Under a fixed discharge of $Q = 20.5$ l/s, two sets of experiments (case 1–case 2) were carried out for two different submerged ratios ($H/D = 0.8$ and 1.2), by varying the water depth from $H = 13$ cm to 19 cm, so that the mean Froude number $Fr = 0.36$–0.53, which is close to Fr_p, meeting the principle of kinematic similarity. Other parameters such as initial channel slope or bedload material gradation were unchanged. Important parameters for both cases are listed in Table 1.

Experimental measurement of bed morphological characteristics over a boulder bed

To investigate the impact of a boulder on bed morphological adjustment, water scour experiments were carried out in an outdoor cement flume with a steep bed slope of 1.25% as

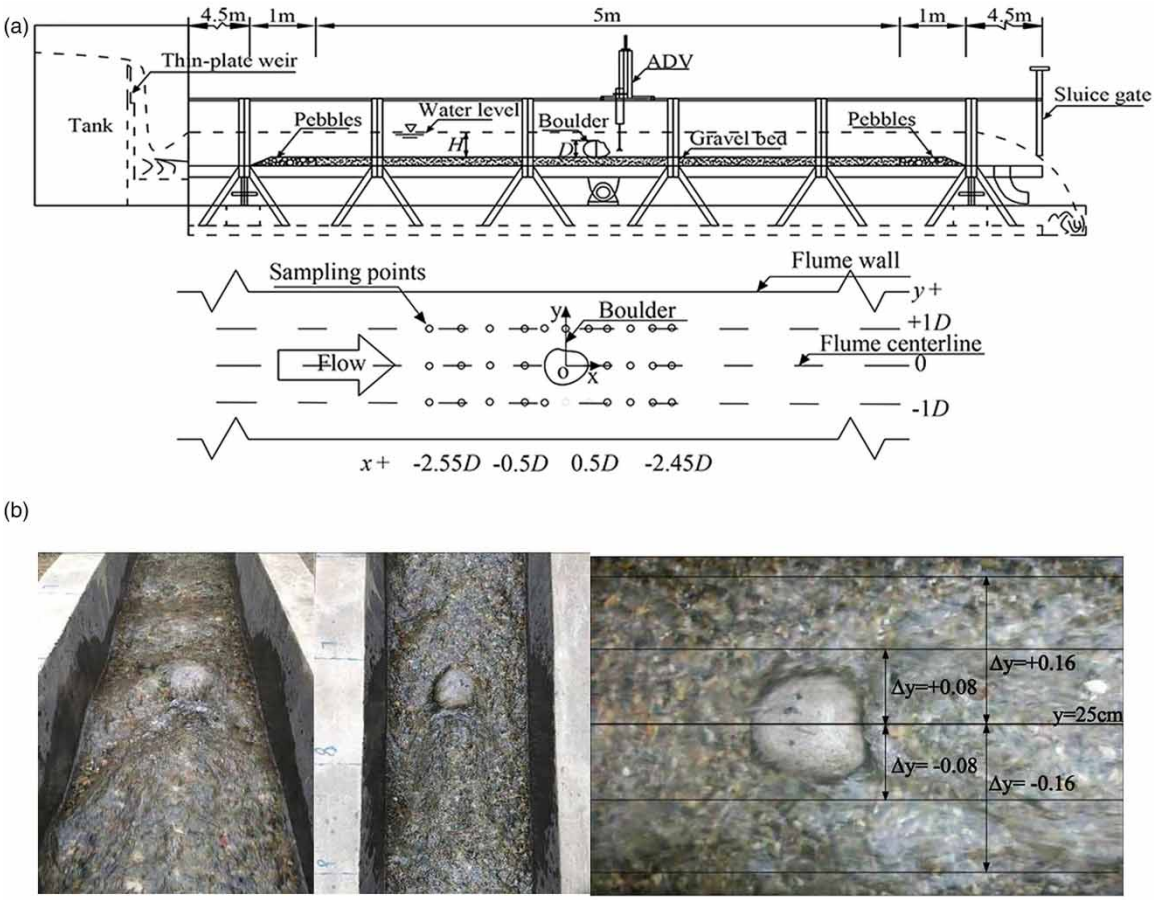

Figure 2 | General arrangements of the boulder bed flow structure experiment: (a) hydrodynamics investigation; (b) bed morphology characteristics investigation.

shown in Figure 2(b). The flume was 4 m long, 0.5 m wide and 0.4 m deep. The boulder used for the last flow experiment was placed on the rough bed so that bed deformation could be generated around the boulder. Bed materials included two main grain sizes: the finer (4–8 mm) was twice the weight of the coarser (10–15 mm) and the median diameter was about $k_s = 7$ mm. Along the experimental reach, 13 cross-sections at an interval of 0.3 m were chosen for flow measurement and coarse pebbles were laid at the inlet.

Overall, initial gravel bed constitutuents, grain size distribution and initial bed surface slope were constant. Three water discharges (Q) were adopted for each group. According to the particle incipient motion velocity (U_e) calculated by the Shamov formula and the measured flow velocity pre-experiment, $Q = 15$ l/s, 20 l/s, 25 l/s

Table 1 | Summary of experiments

Case	H/D	Fr	y^+	x^+	z^+	Number of measuring lines, points	$Re \times 10^3$
1	0.8	0.43–0.53	−1	−4.37	0.318–0.573	12, 74	48–60
			0	−3.5	0.318–0.51	4, 38	
			1	−4.37	0.318–0.573	10, 74	
2	1.2	0.36–0.5	−1	−3.4	0.318–0.892	11, 137	52–72
			0	−5	0.318–0.764	8, 111	
			1	−3.4	0.318–0.924	11, 143	

were determined. To study the impact of the boulder, a no-boulder bed and boulder bed were included in the first two experiments for each group. Meanwhile, upstream sediment feeding was provided on a boulder bed in the third experiment in each group. Therefore, nine cases (i.e. case 3–case 11) of experiments were included to study bed morphological characteristics on boulder beds (see Table 2).

In the case of a boulder bed, a boulder with an effective diameter of $D = 12.3$ cm was embedded in the sediment layer 4–5 cm below the sediment surface. Consequently, the ratio of boulder size to gravel size reached ~23.06, which was close to the geometric ratio from the survey. The size of fed sediment ranged from 4 mm to 8 mm. For the three discharges, sediment of 30 kg was used and the feeding rates were 1 kg, 1.5 kg and 2 kg per two minutes, respectively. When the equilibrium bed morphology was reached, the water level and bed elevation at monitored cross-sections were measured in the following strategy. An electronic total station (ETS) in a local coordinate system was firstly used to measure several locations along the entire reach, referred to as controlling points. Then, the software Agisoft PhotoScan (Kellner & Hubbart 2019) was used to generate 3D spatial data, including the bed elevation, with massive digital images. The ratio of the water depth to the boulder diameter (H/D) was in the range of 0.73–0.89. The Froude number (Fr) along the entire reach was in the range of 0.31–1.05, which reflected the typical flow condition of mountain rivers (Cui & Parker 2005; Zimmermann 2010).

RESULTS

Hydrodynamics around a boulder

Vertical profiles of normalized streamwise velocity (U/u_*) (where u_* = friction velocity), vertical velocity (W/u_*), turbulent kinetic energy TKE/u_*^2 and Reynolds stress $-\overline{u'w'}$ at different positions (upstream, downstream and adjacent to the boulder) were observed for all cases when $H/D = 1.2$ as shown in Figure 2. The ratios $x^+ = x/D$ and $y^+ = y/D$ are referred to as the ratios of the longitudinal and lateral distance from the boulder to the effective size of the boulder; $x^+ = -0$, c, $+0$ indicates the leading edge, center and trailing edge of the boulder.

Figure 3(a) shows that located one diameter away from the boulder centerline ($y^+ = \pm 1$), the vertical profile of streamwise velocity (U/u_*) approximately complies with the logarithmic law (Nezu *et al.* 1994). Clear deviations happen in the regions of $x^+ = -0.64$–0.32, where the magnitudes of U/u_* are reduced. A possible cause is that the boundary effect of the boulder plays a resistant role in velocity development. However, a different pattern of the vertical profile of U/u_* can be observed at the boulder centerline ($y^+ = 0$). The U/u_*-profile in the vicinity of the boulder ($x^+ = 0.32$–2.55) deviates highly from the standard logarithmic law, owing to the blockage of the boulder. This effect is more pronounced for regions at the downstream of the boulder. Especially, the streamwise velocity tends to increase vertically above the boulder top level ($z^+ = 1$), assembling an inflection in the velocity profile.

Table 2 | Summary of water scour experiments

Case	Q(l/s), H/D	Boulder size D (cm)	Feeding sediment size d (mm)	Feeding rate, feeding duration, and total amount	Fr
3	15, 0.73	–	–	–	0.60–0.74
4	15, 0.73	12.3	–	–	0.47–1.02
5	15, 0.73	12.3	4–8	1 kg/2 min, 60 min, 30 kg	0.31–0.96
6	20, 0.81	–	–	–	0.69–0.88
7	20, 0.81	12.3	–	–	0.47–0.86
8	20, 0.81	12.3	4–8	1.5 kg/2 min, 40 min, 30 kg	0.44–0.94
9	25, 0.89	–	–	–	0.74–0.85
10	25, 0.89	12.3	–	–	0.50–1.05
11	25, 0.89	12.3	4–8	2 kg/2 min, 30 min, 30 kg	0.51–0.78

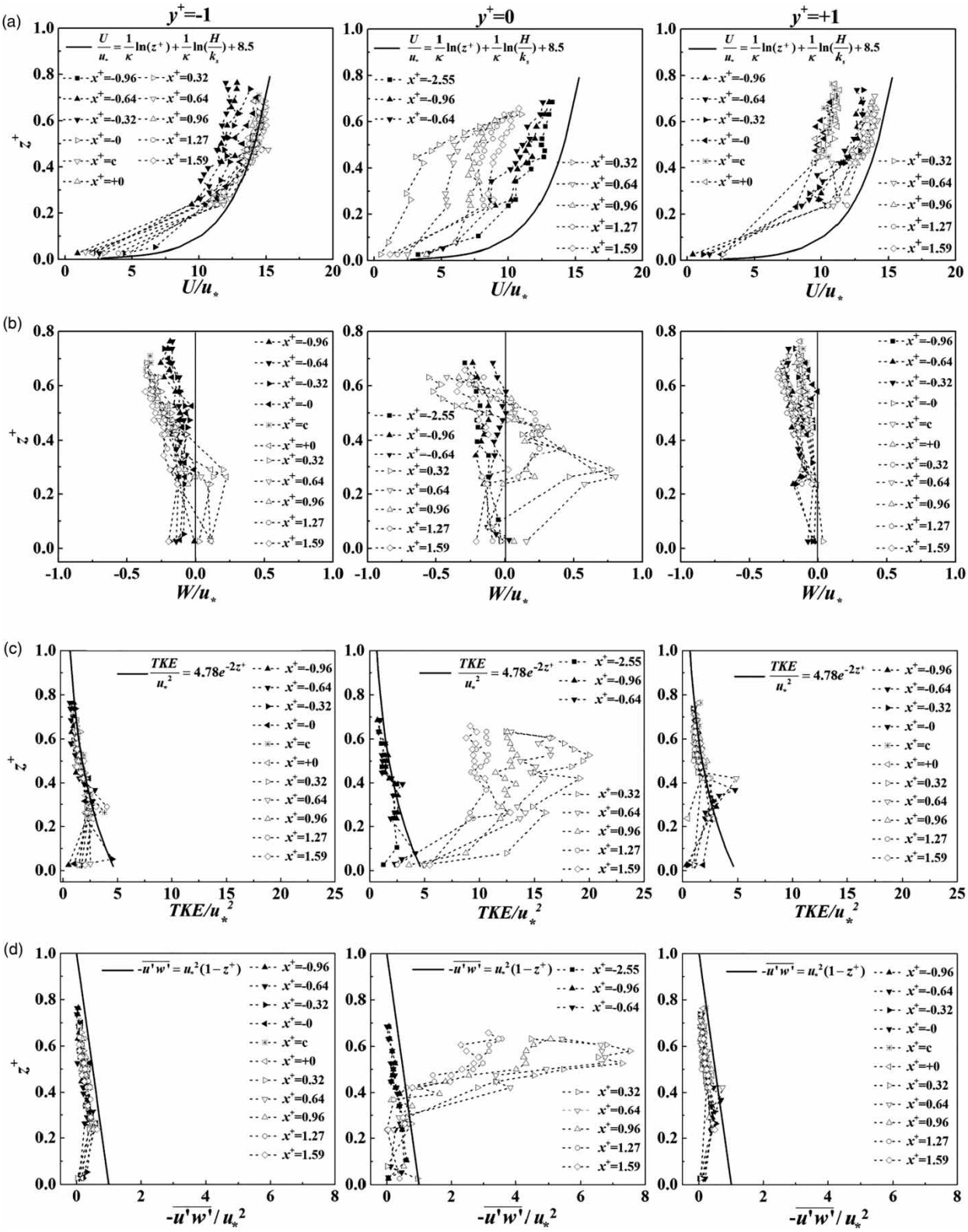

Figure 3 | Distributions of normalized (a) streamwise velocity U/u_*, (b) vertical velocity W/u_*, (c) turbulent kinetic energy TKE/u_*^2 and (d) Reynolds stress $-\overline{u'w'}$ when $H/D = 1.2$.

Moreover, below the boulder top level, the streamwise velocity is dramatically deflected compared with its counterpart in the upstream, indicating potential sediment deposition in the wake region of the boulder.

For the vertical velocity (W/u_*) (see Figure 3(b)), W/u_* for the three transects are generally negative at the upstream ($x^+ = -0.96$–c), which indicates the generation of downflow when the water body encounters the boulder. The generated downflow is broadly observed when flow passes obstacles like bridge piles (Unger & Hager 2007). At the downstream, the difference in the pattern of W/u_* can be observed between the centerline and side transects. In the wake region of the boulder, W/u_* is positive at the lower layer ($z^+ < 0.4$) and negative at the upper layer ($z^+ > 0.4$), but in the adjacent regions, W/u_* remains negative over the entire water depth. Note that the pattern on the left side and right side does not match, probably owing to the non-complete symmetry of the boulder in the experiment. The pattern difference essentially indicates the flow circulation formed at the downstream. The maximum magnitude of W/u_* roughly attains 7% of the primary flow velocity (U/u_*). This is much greater than those from flow circulations in compound channels (Tominaga & Nezu 1991) and partly vegetated channels (Choi & Kang 2006). This implies a stronger transverse sediment motion in the boulder-obstructed channel than that in other geometrically irregular channels.

Vertical Reynolds stress and turbulent kinetic energy (*TKE*) at different locations around the boulder are shown in Figure 3(c). Here, parameters are normalized by u_*^2. On both sides of the boulder ($y^+ = \pm 1$), the vertical distribution of TKE/u_*^2 over the boulder-bed complies with the decaying power law (Nezu *et al.* (1994)) over the water depth. However, significant difference occurs at the center transect ($y^+ = 0$). At the upstream of the boulder, the decaying power law is valid, while the *TKE* increases significantly over the water depth in the wake regions of the boulder (downstream). The peak magnitudes occur at $x^+ = 0.32$, which is the nearest one among the downstream longitudinal locations. Further downstream, despite obvious reduction, the *TKE* remains at a relatively great level. The pronounced *TKE* downstream of the boulder is attributed to large-scale vortices generated in the wake region.

Figure 3(d) illustrates vertical profiles of Reynolds shear stress *RSS* ($-\overline{u'w'}$) at different x^+ (relative to the mass density ρ of fluid). On both lateral sides ($y^+ = \pm 1$), $-\overline{u'w'}$ suggests the same pattern as the *TKE* that firstly they increase as vertical distance z^+ decreases, up until reaching a maximum value at around $z^+ = 0.2$–0.4; they then decrease with z^+ to return to relatively small values. This characteristic also indicates that bed shear stress beyond one diameter of the boulder shows consistency with that over the flat bed. In the central transect ($y^+ = 0$), the upstream *RSS* ($z^+ < -0.64$) are roughly maintained within a small range of 0–1. After the boulder, they become overall greater than that on both sides as well. Still, those maximum values occur at $x^+ = 0.32$ and others remain at great levels above $z^+ = 0.4$. However, the vertical profiles of *RSS* no longer fit the logarithmic law. Moreover, *RSS* over the u–w direction gradually decreases as x^+ increases, characterizing a recovery of undisturbed turbulent intensities. Therefore, in the wake regions of the boulder, the deflected mean flow field enables the deposition of sediment but the significantly increased turbulent flow field enables the possibility of surface sediment resuspension.

Bed morphological characteristics impacted by a boulder

Water scour experiments were conducted to investigate the bed morphological characteristics in terms of gravel bed only, gravel bed with a boulder and gravel bed with a boulder and sediment feeding. These experiments are anticipated to be able to provide insights into how a boulder impacts the bed morphological change. Firstly, bed morphology indicated by the bed elevation change (Δz) contour throughout the equilibrium bed is shown in Figure 4, presenting an overall pattern of bed morphology. In the presence of a boulder, bed elevation around the boulder is comparatively lower than in other regions due to significant local bed scour, forming a pool region. In the near-wake region after the boulder, the bed morphology occurs with an obvious central deposition zone of relatively higher elevation and gullies on both sides. This deposition region in the central flume is referred to as riffle, corresponding to the upstream pool region around the boulder. Due to the irregular shape of the boulder, the downstream bed morphology evidently exhibits a pattern of left low and right high. This evolution pattern is similar to a result observed

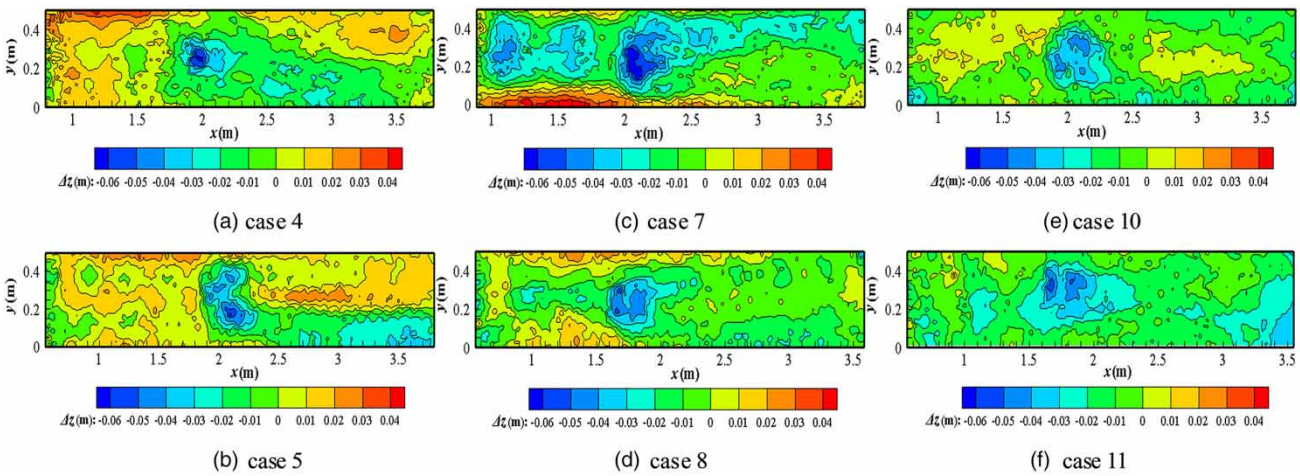

Figure 4 | Elevation maps in the entire channel for all experimental runs. Red parts represent higher elevation and blue parts represent relatively lower elevation. Dashed oval circles in the graph represent the deposition zone on the lee side of the boulder. Please refer to the online version of the paper to see this figure in color: http://dx.doi.org/10.2166/ws.2019.175.

by Shamloo *et al.* (2001) that on a boulder bed, erosion often occurs with a scouring hole around the boulder but with gullies on both sides downstream of the boulder.

A more quantitative description of the bed morphology characteristics can be addressed by the longitudinal bed profile along the boulder centerline as shown in Figure 5. It is clearly observed that in the absence of a boulder, general bed degradation occurs under different water discharges. An increasing discharge tends to result in greater degradation. In the presence of a boulder, the bed profile can be divided into several segments with constant slopes represented by i_{wb} and i_{wbs} in the cases of no sediment feeding and sediment feeding. A scour pool can be clearly observed around the boulder, following which a high-level riffle exists downstream. Two such bed morphological features constitute a pool–riffle sequence. However, with upstream sediment feeding, the bed topography differs a lot from its counterpart without upstream sediment feeding. When sediment is supplied at the upstream, moving sediment can partially compensate for the original bed materials which are eroded downstream. Consequently, the bed topography in the presence of sediment feeding is generally higher than that in the absence of sediment feeding. Therefore, the pool region becomes shallower and the riffle region becomes higher in the presence of sediment feeding. In addition, this tendency is stronger when the water discharge is smaller ($Q = 15$ l/s and 20 l/s). However, an exception occurs for the highest water discharge, under which the bed topography in the presence of sediment feeding is slightly lower than that in the absence of sediment feeding.

As indicated by Figure 6, it is rationally expected that the characteristic bed morphologies (i.e., pool and riffle) might be substantially related to the flow condition and the geometry boundary. Thus two length scales (L_1 and L_2) which are associated with the geometries of pool and riffle are defined as shown in Figure 6(a). In addition, the distance (S) between the pool and riffle is regarded as a characteristic geometric scale. Two scenarios are proposed according to flume observations. It is simple to know that the riffle is below the initial bed elevation when $L_1 > L_2$ and above the initial bed elevation when $L_1 > L_2$. Figure 6(b) presents the results for different flow configurations. Clearly, the two length scales (normalized by D) are comparable for all cases, except for case 5 in which the flow rate is relatively small (15 l/s) and the sediment feeding is present. The length scale of the riffle (L_2/D) is much greater than that of the pool (L_1/D), indicating the bed aggradation. The cause might be that the bed shear arising from the stream power in that case is lower than the significant form drag force by the riffle.

To further analyze the relationship between the length scales of pool and riffle and flow configurations, length scales (L_1/D and L_2/D) are plotted against the Froude number in terms of the location of the boulder (Fr_b). As shown in Figure 7(a), it can be clearly seen that both L_1/D and L_2/D increase as the Froude number increases and no

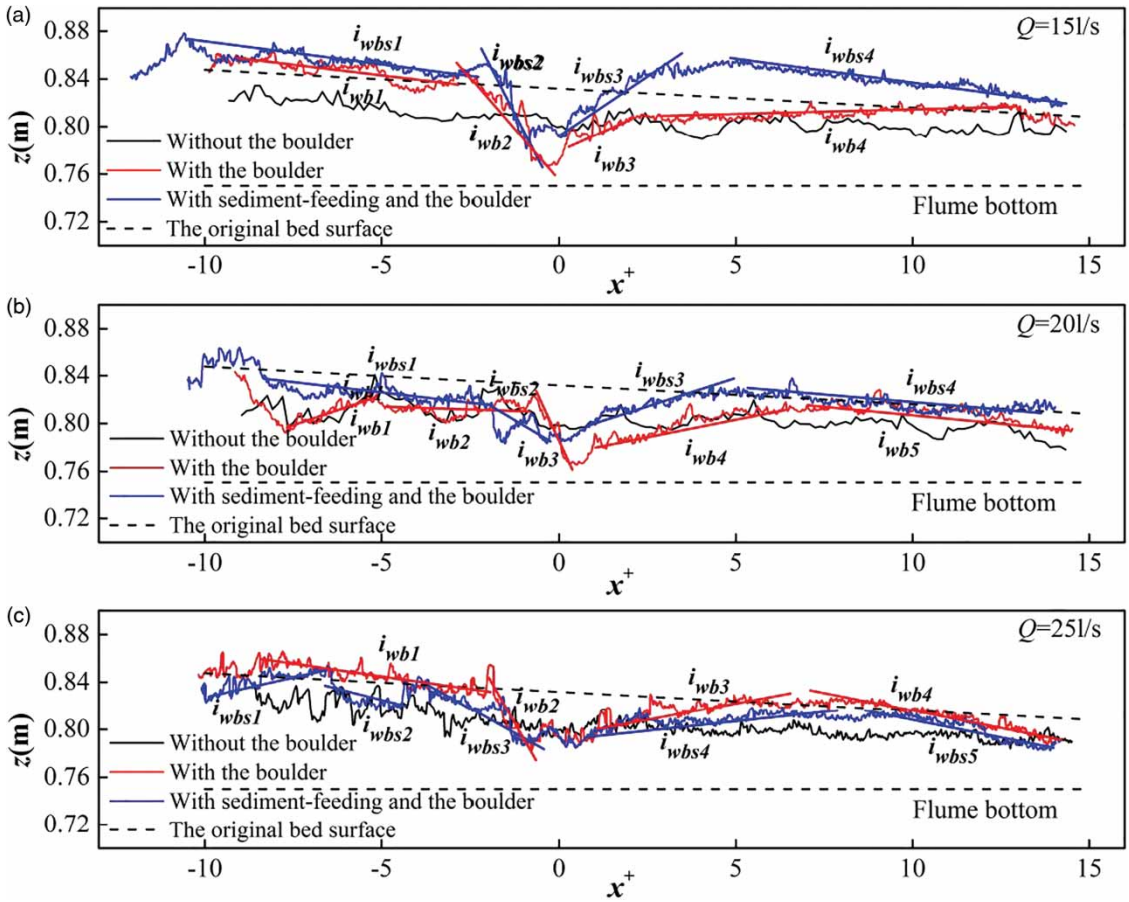

Figure 5 | Deformed longitudinal topography in the profile of $y = 0.25$ (centerline) under three configurations: (1) without the boulder; (2) with the boulder; (3) with the boulder and sediment-feeding; i_{wb} and i_{wbs} represent the general slopes along the flume under configurations (2) and (3) respectively.

apparent difference occurs because of the sediment feeding. By fitting, all data can approximately fall onto a linear curve with a relative high fitting coefficient. Still, an apparent deviation occurs in terms of the riffle length scale for case 5, which shows a large riffle length scale against a small Froude number. This corresponds to pool–riffle morphology scenario 1 described in the definition. Figure 7(b) shows the relation between the normalized distance S/D and Fr_b. Likewise, most data can be observed to fall onto a linear curve in spite of acceptable bias. Similar to the above length scales of pool and riffle, the distance between the pool and riffle increases as the Froude number increases. An apparent biased point can be observed which corresponds to the biased point of the length scale in Figure 7(a). The pair of biased points compared with other points for the length scale of riffle and pool–riffle distance may suggest another pattern of scaling relation accounting for pool–riffle morphology scenario 1.

Similarly, the net bed erosion volume (degraded bed volume minus aggraded bed volume in terms of the initial bed) is calculated, and it is plotted against the mean Froude number for the entire bed in Figure 7(c). For convenience, the mean Froude number (Fr) is interpreted as the stream power. It is likely that linear relations can be identified between the net bed erosion volume and mean Froude number. In the absence of a boulder, the net bed erosion linearly increases with the mean Froude number, which indicates that the riverbed generally degrades more with a higher stream power. However, when the boulder is present, an opposite relation can be observed. This phenomenon is interesting because the presence of the boulder tends to induce more significant bed scour as indicated by the

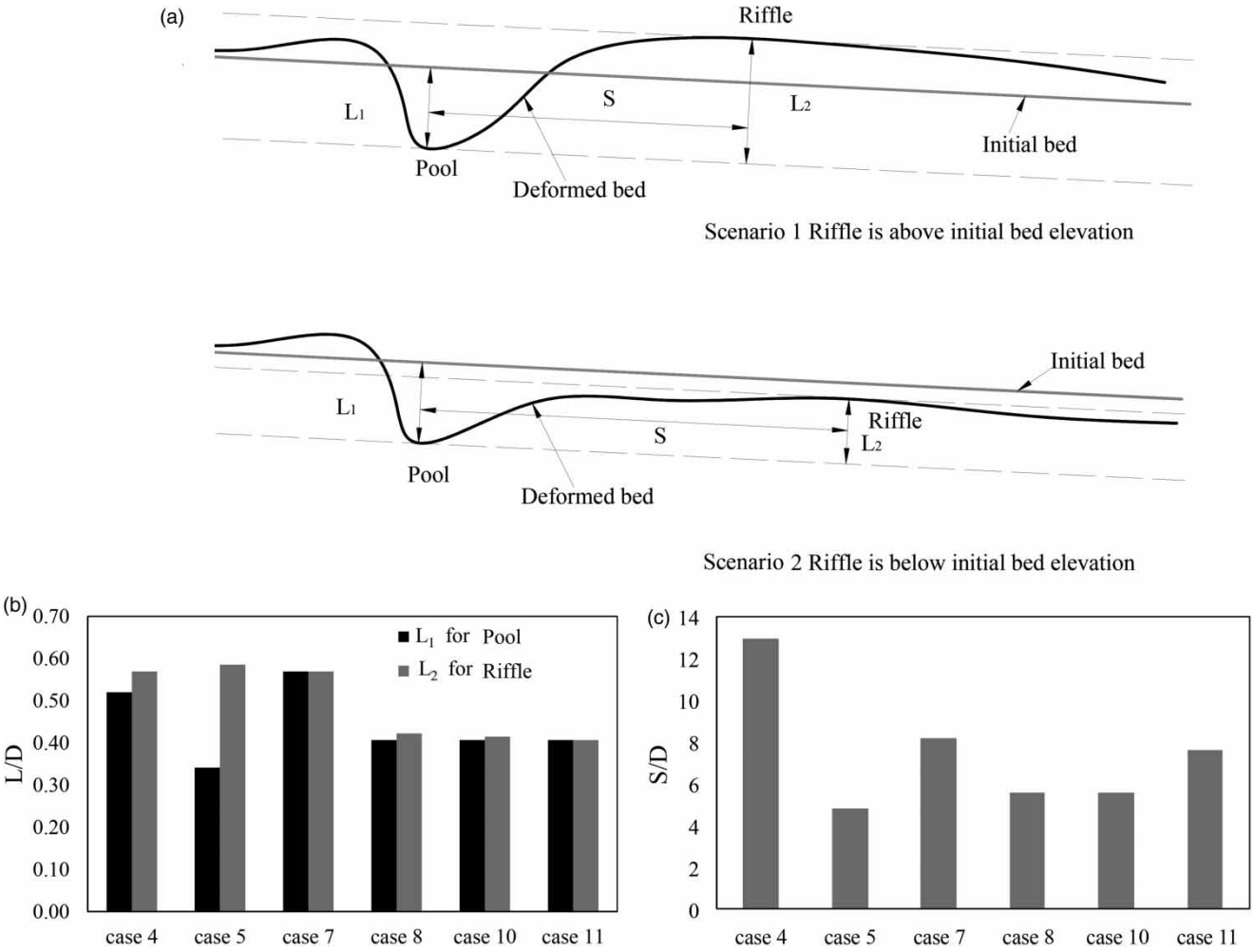

Figure 6 | (a) Calculation framework of characteristic lengths of pool and riffle, (b) length scales (L_1 and L_2) and (c) normalized distance (S/D) in different cases.

increase in pool length scale with the increasing boulder-related Froude number (see Figure 6(b)). In fact, more scour also results in more downstream deposition unless the stream power is large enough to erode all downstream bed materials. Therefore, it is reasonable that net bed erosion can decrease with increasing mean stream power. Interestingly, the biased effect observed in Figure 6(a) and 6(b) disappears in this relation.

CONCLUSIONS

Large-size boulders widely existing in mountain rivers play significant roles in impacting local hydrodynamics and morphodynamics around the boulders themselves. In the presented study, two sets of experiments were conducted to investigate those impacts.

The first set of experiments examined the hydrodynamics around the boulder over a gravel bed, providing a fundamental background for understanding the flow–boulder interaction. In this section, the spatial distribution of flow characteristics at the upstream and downstream of the boulder at three different transverse locations was discussed. Results show that on lateral sides of the boulder ($y/D = 1$ or -1), the existence of the boulder only has a slight impact on the mean flow characteristics, and flow behaviors over a hydraulically rough bed are still applicable. Specifically, the vertical profile of longitudinal velocity

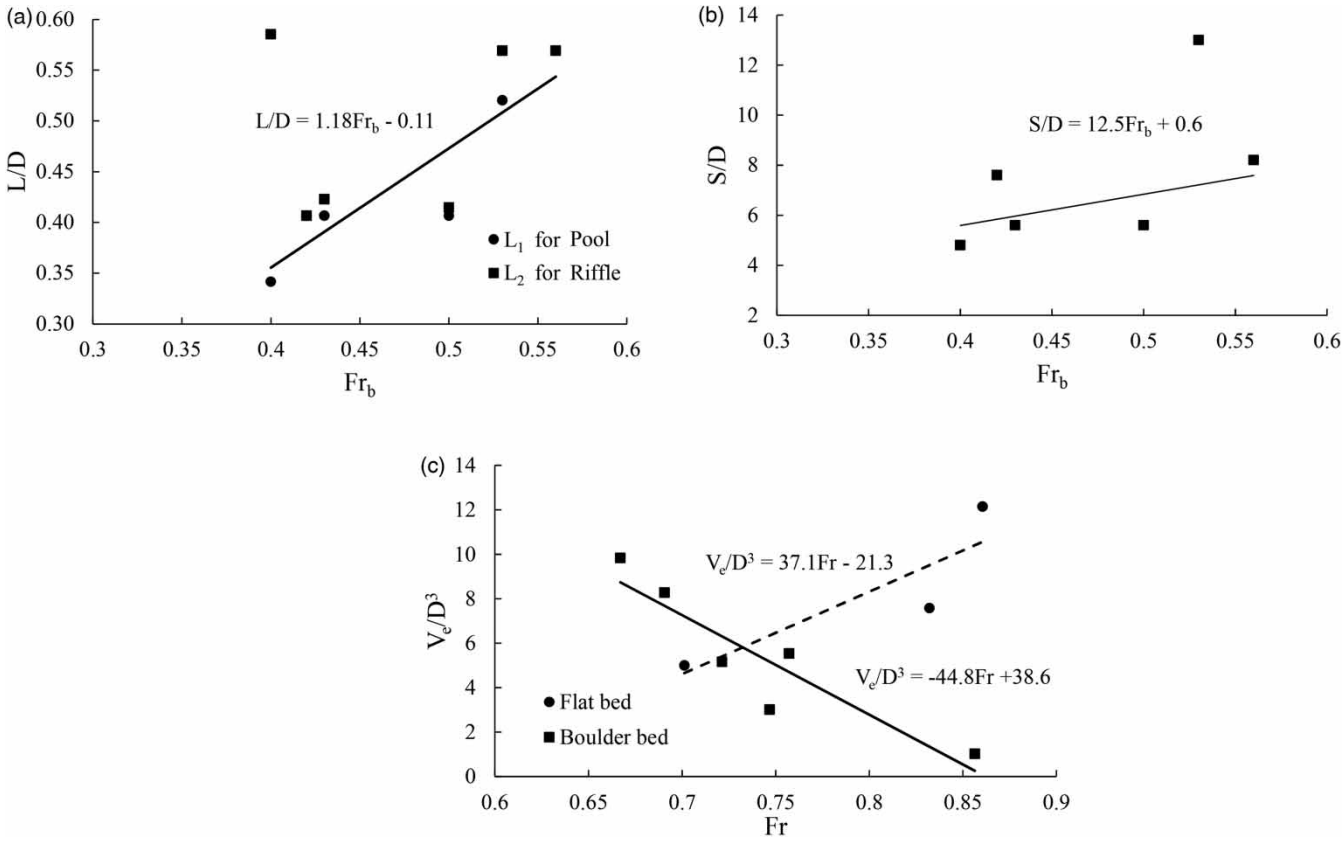

Figure 7 | Relationship between geometric features of the pool–riffle sequence system and hydrodynamics around a boulder: (a) length scales of the pool and riffle (L_1/D and L_2/D) as a function of the boulder-related Froude number (Fr_b); (b) normalized pool–riffle distance (S/D) as a function of the boulder-related Froude number (Fr_b); (c) net bed erosion volume (V_e) as a function of the mean flow Froude number (Fr).

follows the logarithmic law, the vertical Reynolds stress follows the linear decay curve and the turbulent kinetic energy (*TKE*) follows the decay power function suggested by Nezu *et al.* (1994). At the transect of the boulder centerline ($y/D = 0$), the flow is clearly deflected by the boulder while turbulent characteristics in the horizontal dimension are enhanced in the wake of the boulder, which is caused by the generation of horizontal vortices. The increase in the vertical Reynolds stress at the upper layer is owing to water flow overtopping the boulder possibly resulting in vertical large-scale vortices.

In the second set of experiments, water scour experiments were carried out over a steep bed slope, which is common in mountain rivers. Three types of boundaries were designed, including one in which the boulder was absent, one in which the boulder was present without upstream sediment feeding and one in which both the boulder and upstream sediment feeding were present. Over the steep slope, sediment can be initiated for all configurations, while the curve of accumulated collected sediment at the exit shows the difference for each configuration. During experiments, significant scour occurred around the boulder and bedloads were transported downstream, generating the typical pool–riffle sequence. It is identified that two scenarios of riffles can exist in regard to the initial bed elevation. The analysis of the geometric scale of pool and riffle shows that two length scales of pool and riffle and distance between the pool and riffle are positively related to the Froude number in terms of the boulder location (Fr_b) in a linear relation $L/D = 1.18Fr_b - 0.11$ and $S/D = 12.5Fr_b + 0.6$. The scenario in which the generated riffle is above the initial bed elevation, interestingly, has a difference from the observed relation. However, the net bed erosion volume is found to be negatively related to the mean Froude number (Fr) in a linear relation for both

scenarios $V_e/D^3 = -44.8Fr - 38.6$, differing from the high bed degradation with high Fr in the absence of the boulder $V_e/D^3 = 37.1Fr - 21.3$.

ACKNOWLEDGEMENTS

This research was supported by the National Key R&D Program of China (2016|YFC0402304, 2017YFC1502504 and 2018YFC1505402) and the National Natural Science Foundation of China (51579163 and 41771543).

REFERENCES

Afzalimehr, H., Maddahi, M. R., Naziri, D. & Sui, J. 2019 Effects of non-submerged boulder on flow characteristics – a field investigation. *International Journal of Sediment Research* **34** (2), 136–143.

Baki, A. B. M., Zhu, D. Z. & Rajaratnam, N. 2014 Mean flow characteristics in a rock-ramp-type fish pass. *Journal of Hydraulic Engineering* **140** (2), 156–168.

Baki, A. B. M., Zhu, D. Z. & Rajaratnam, N. 2015 Turbulence characteristics in a rock-ramp-type fish pass. *Journal of Hydraulic Engineering* **141** (2), 04014075.

Baki, A. B. M., Zhang, W., Zhu, D. Z. & Rajaratnam, N. 2016 Flow structures in the vicinity of a submerged boulder within a boulder array. *Journal of Hydraulic Engineering* **143** (5), 04016104.

Barry, J. J., Buffington, J. M. & King, J. G. 2004 A general power equation for predicting bed load transport rates in gravel bed rivers. *Water Resources Research* **40** (10), W10401.

Cameron, S. M., Nikora, V. I. & Stewart, M. T. 2017 Very-large-scale motions in rough-bed open-channel flow. *Journal of Fluid Mechanics* **814**, 416–429.

Cao, Z. 1997 Turbulent bursting-based sediment entrainment function. *Journal of Hydraulic Engineering* **123** (3), 233–236.

Chiari, M. & Rickenmann, D. 2011 Back-calculation of bedload transport in steep channels with a numerical model. *Earth Surface Processes and Landforms* **36** (6), 805–815.

Choi, S.-U. & Kang, H. 2006 Numerical investigations of mean flow and turbulence structures of partly-vegetated open-channel flows using the Reynolds stress model. *Journal of Hydraulic Research* **44** (2), 203–217.

Cui, Y. & Parker, G. 2005 Numerical model of sediment pulses and sediment-supply disturbances in mountain rivers. *Journal of Hydraulic Engineering* **131** (8), 646–656.

Galia, T. & Hradecký, J. 2011 Bedload transport and morphological effects of high-magnitude floods in small headwater streams – Moravskoslezské Beskydy Mts. (Czech Republic). *Journal of Hydrology and Hydromechanics* **59** (4), 238–250.

Ghilardi, T. 2013 Experimental study on bedload pulses in a steep flume with boulders. In: *35th IAHR World Congress, John Fisher Kennedy Student Paper Competition*, TPU, Chengdu, China.

Ghilardi, T. 2014 *Sediment Transport and Flow Conditions in Steep Rivers with Large Immobile Boulders*. Communication 58, EPFL/LCH, Lausanne, Switzerland.

Habersack, H. M. & Laronne, J. B. 2002 Evaluation and improvement of bed load discharge formulas based on Helley–Smith sampling in an alpine gravel bed river. *Journal of Hydraulic Engineering* **128** (5), 484–499.

Hassan, M. A. & Church, M. 2000 Experiments on surface structure and partial sediment transport on a gravel bed. *Water Resources Research* **36** (7), 1885–1895.

Kellner, E. & Hubbart, J. A. 2019 A method for advancing understanding of streamflow and geomorphological characteristics in mixed-land-use watersheds. *Science of The Total Environment* **657**, 634–643.

Lacey, R. W. J. & Roy, A. G. 2006 Turbulent wake region of large roughness elements: combining flow visualization and high frequency velocity measurements. In: *River Flow 2006* (R. M. L. Ferreira, E. C. T. L. Alves, J. G. A. B. Leal & A. H. Cardoso, eds), Taylor & Francis, London, UK, pp. 125–134.

Lacey, R. W. J. & Roy, A. G. 2008 Fine-scale characterization of the turbulent shear layer of an instream pebble cluster. *Journal of Hydraulic Engineering* **134** (7), 925–936.

Lenzi, M. A., Mao, L. & Comiti, F. 2006 When does bedload transport begin in steep boulder-bed streams? *Hydrological Processes* **20** (16), 3517–3533.

Nezu, I., Nakagawa, H. & Jirka, G. H. 1994 Turbulence in open-channel flows. *Journal of Hydraulic Engineering* **120** (10), 1235–1237.

Nitsche, M., Rickenmann, D., Turowski, J. M., Badoux, A. & Kirchner, J. W. 2011 Evaluation of bedload transport predictions using flow resistance equations to account for macro-roughness in steep mountain streams. *Water Resources Research* **47** (8), W08513.

Papanicolaou, A. N., Bdour, A. & Wicklein, E. 2004 One-dimensional hydrodynamic/sediment transport model applicable to steep mountain streams. *Journal of Hydraulic Research* **42** (4), 357–375.

Papanicolaou, A. N., Kramer, C. M., Tsakiris, A. G., Stoesser, T., Bomminayuni, S. & Chen, Z. 2012 Effects of a fully submerged boulder within a boulder array on the mean and turbulent flow fields: implications to bedload transport. *Acta Geophysica* **60** (6), 1502–1546.

Papanicolaou, A. N., Tsakiris, A. G., Wyssmann, M. A. & Kramer, C. M. 2018 Boulder array effects on bedload pulses and depositional patches. *Journal of Geophysical Research: Earth Surface* **123** (11), 2925–2953.

Rickenmann, D. 2001 Comparison of bed load transport in torrents and gravel bed streams. *Water Resources Research* **37** (12), 3295–3305.

Schneider, J. M., Rickenmann, D., Turowski, J. M., Bunte, K. & Kirchner, J. W. 2015 Applicability of bed load transport models for mixed-size sediments in steep streams considering macro-roughness. *Water Resources Research* **51** (7), 5260–5283.

Shamloo, H., Rajaratnam, N. & Katopodis, C. 2001 Hydraulics of simple habitat structures. *Journal of Hydraulic Research* **39** (4), 351–366.

Strom, K. B., Papanicolaou, A. N. & Constantinescu, G. 2007 Flow heterogeneity over 3D cluster microform: laboratory and numerical investigation. *Journal of Hydraulic Engineering* **133** (3), 273–287.

Tominaga, A. & Nezu, I. 1991 Turbulent structure in compound open-channel flows. *Journal of Hydraulic Engineering* **117** (1), 21–41.

Unger, J. & Hager, W. H. 2007 Down-flow and horseshoe vortex characteristics of sediment embedded bridge piers. *Experiments in Fluids* **42** (1), 1–19.

Yager, E. M., Kirchner, J. W. & Dietrich, W. E. 2007 Calculating bed load transport in steep boulder bed channels. *Water Resources Research* **43** (7), W07418.

Yager, E. M., Dietrich, W. E., Kirchner, J. W. & McArdell, B. W. 2012 Prediction of sediment transport in step–pool channels. *Water Resources Research* **48** (1), W01541.

Zimmermann, A. 2010 Flow resistance in steep streams: an experimental study. *Water Resources Research* **46**, 9, W09536.

Zimmermann, A. & Church, M. 2001 Channel morphology, gradient profiles and bed stresses during flood in a step–pool channel. *Geomorphology* **40** (3–4), 311–327.

First received 31 August 2019; accepted in revised form 31 October 2019. Available online 27 November 2019